Available online at www.sciencedirect.com
ScienceDirect
Physica B 394 (2007) 46–55
PHYSICA B
www.elsevier.com/locate/physb

The hydraulic jump and ripples in liquid helium

E. Rolley[a,*], C. Guthmann[a], M.S. Pettersen[b]

[a]Laboratoire de Physique Statistique de l'ENS, associé au CNRS et aux Universités Paris 6 et Paris 7, 24 rue Lhomond, 75005 Paris, France
[b]Washington and Jefferson College, 60 S. Lincoln St., Washington, PA 15301, USA

Received 26 September 2006; received in revised form 23 January 2007; accepted 6 February 2007

Abstract

We have studied the characteristics of the circular hydraulic jump using liquid helium. Surprisingly, the radius of the jump does not change at the superfluid transition. We think that the flow is still dissipative below the lambda point because the velocity exceeds the critical one. The jump radius R_j is compared with various models. In our parameter range, we find that the jump can be treated as a shock, and that capillary effects are important. Below the superfluid transition, we observed a standing capillary wave between the impact of the jet and the jump. Assuming that the superfluid flow can be described with an effective viscosity, we calculate the wave vector and thus obtain the value of the liquid thickness, which is in reasonable agreement with predictions. However, the spatial variation of the wave amplitude depends much more strongly on temperature than we calculate.

PACS: 47.35+i; 47.15.Fe; 47.37.+q; 67.40.Bz

Keywords: Hydraulic jumps; Superfluid; Helium; Capillary wave

1. Introduction

When a jet of liquid hits a flat surface, there may occur a sharp increase in the depth h of the fluid layer at some radius R_j from the center of the jet, as shown schematically in Fig. 1. This is called the hydraulic jump. (By continuity, there is a corresponding decrease in the average fluid velocity outside the jump.) The hydraulic jump is easily observed in any sink, and has become a popular undergraduate experiment [1,2]. Many experiments have been carried out in the past 50 years (see references in Ref. [3]), mainly with ordinary fluids like water or ethylene glycol.

The primary interest in using liquid helium to study the hydraulic jump lies in its remarkable quantum properties at low temperature. Above the superfluid transition temperature $T_\lambda = 2.17\,\mathrm{K}$, helium behaves as an ordinary liquid, though with a very small kinematic viscosity ($\nu \approx 2\times 10^{-8}\,\mathrm{m^2/s}$), and high Reynolds number ($Re \sim 2\times 10^4$) can be obtained easily. Below T_λ, the liquid behaves as a mixture of a normal fluid and a superfluid component, which can flow without dissipation; hence there is some hope that using liquid helium one can observe the hydraulic jump in an inviscid fluid [4], which should have quite a different jump radius R_j, as originally calculated by Rayleigh (see Section 3.1 below).

The second important feature of our experiment is its size: typical values of R_j are in the millimeter range, one or two orders of magnitude smaller than in previous experiments. This should increase the effect of the surface tension, which is expected to decrease R_j [5], as will also be explained in Section 3.1.

The experimental setup is described in Section 2. In Section 3.1, we review the theoretical work which has been done on the jump. In Section 3.2 we present our measurements of the radius R_j as a function of the flow rate Q and depth d of the normal fluid outside the jump. We find that the measured values R_j lie between the values predicted with and without the effects of surface tension. A short preliminary report of these measurements has been published elsewhere [6]. Then we describe in Section 3.3 what happens at the superfluid transition. Surprisingly, R_j

*Corresponding author.
E-mail address: rolley@lps.ens.fr (E. Rolley).

0921-4526/$ - see front matter © 2007 Elsevier B.V. All rights reserved.
doi:10.1016/j.physb.2007.02.006

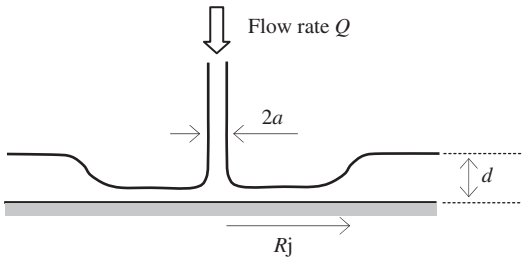

Fig. 1. Hydraulic jump.

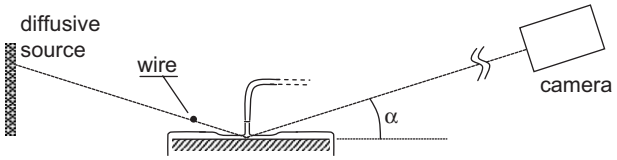

Fig. 2. Setup.

Table 1
Physical properties of liquid helium (after [7])

T (K)	ν (10^{-8} m^2/s)	ρ_L (g/cm^3)	γ (mN/m)	L_C (mm)
4.2	2.59	0.125	8.88	0.266
3	2.52	0.141	21.55	0.394
2.45	2.14	0.145	26.99	0.437
1.5	0.88[a]	0.145	33.22	0.480

[a]Effective viscosity (see text).

does not change much at the transition temperature; we show that this is probably due to the fact that the flow is supercritical. Assuming that the whole fluid behaves as an ordinary fluid with a viscosity equal to that of the normal fluid component, we find that the data below the superfluid transition are consistent with the ones above the transition. The only specific feature of the low temperature regime is the appearance of developed capillary waves in the thin film region. In Section 4, we discuss the dispersion relation of the ripples, and we use their wave length to estimate the thickness of the flowing film for comparison with various models. Finally, we comment on the decay length of the ripples, which unlike R_j does appear to be affected by the superfluid transition.

2. Experimental setup

The experiments are performed in an optical helium-4 cryostat. The experimental cell is positioned in the vacuum below the main helium-4 bath; the thermal contact between the bath and the cell is achieved by a solid copper piece. A schematic view of the setup is shown in Fig. 2. The liquid jet hits a horizontal optical mirror positioned at the center of the experimental cell. Usually, the mirror is illuminated by diffusive source, and a side view is obtained by means of a CCD camera equipped with a macro objective. The observation angle with respect to the horizon is set to $\alpha = 12.5°$. An auxiliary mirror, positioned above the main one, allows observation of the jump from above, at normal incidence. This is useful for checking that the jump is circular.

The helium forming the jet is admitted into the cryostat from a high pressure vessel, and condenses in three successive heat exchangers in the main helium-4 bath. The flow rate Q is regulated with an accuracy of 1% by means of a flowmeter operating at room temperature. The range of Q is 2–100 mm^3/s. At lower flow rate, the jet is unstable and often intermittent, especially below the superfluid transition; at higher flow rate, thermalization of the incoming fluid is not sufficient. The temperature of the cell can be set between 4.2 and 1.5 K by pumping the main He bath (the superfluid transition occurs at 2.17 K under saturated vapor pressure). In this range of flow rate and temperature, no thermocapillary Marangoni flow is expected to arise. The values of the parameters of interest at the temperatures where measurements were performed are summarized in Table 1.

The final part and the outlet of the helium line is made of a Cu–Ni capillary, whose inner diameter is of the order of 0.2 mm. The end of the capillary has been polished, and looks perfectly circular under a microscope. However, at high flow rate, the jump is not perfectly circular (deviations are of the order of 5%); this may be due to small defects of the tube, or possibly to an incipient instability of the jump [8]. The height of the end of the tube with respect to the mirror was varied between 2.5 and 1 mm. This has a small effect on a (which is always very close to 0.1 mm), and on R_j.

The radius of the impinging jet a and R_j are easily measured on the images. R_j lies in the range 0.4 to 4 mm, much smaller than the mirror radius (24 mm). In order to measure d, we have used an original technique. A small wire is held parallel to the mirror and perpendicular to the camera axis, at a position such that its image reflected by the mirror goes through the center of the mirror, as shown in Fig. 3. When a layer of liquid of thickness d is present on the mirror, the image becomes double. One of the images corresponds to rays reflected from the free surface; it is very faint since the refraction index of the liquid is close to the one of the vapor ($n_L - n_V \approx 0.028$). The second image corresponds to rays reflected from the mirror; since these rays are refracted at the free surface, the second image is shifted upwards by a quantity $\delta = d/(2\cos\alpha(1 - \tan\alpha\tan r))$, where $n_L \sin r = n_V \cos\alpha$. The ratio δ/d depends on the temperature through the refractive indices. For $\alpha = 12.5°$, one finds $\delta/d = 0.552$ and 0.657 at $T = 4.2$ and 1.5 K, respectively. As d is of the order of 100 μm, the shift is of the order of a few pixels. This is small, but sub-pixel resolution can be easily achieved using standard image analysis, and the final accuracy of the liquid thickness is of the order of 10%. The thickness in the fast flow region can only be measured when the flow is very

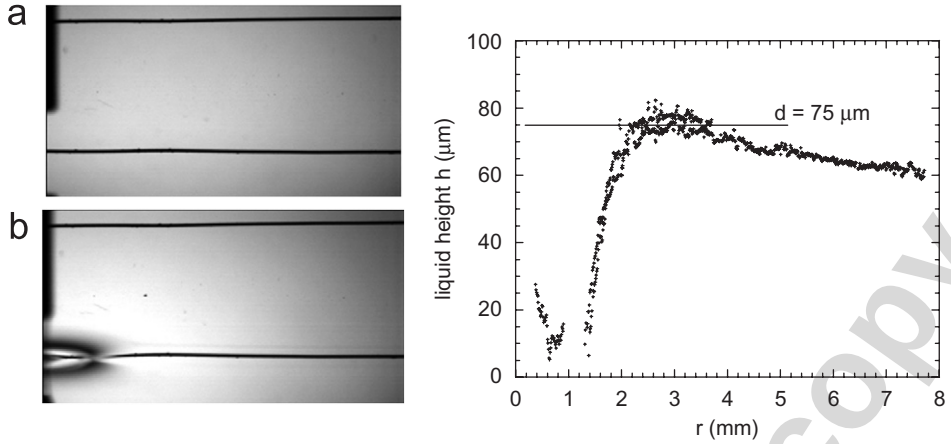

Fig. 3. Measurement of the liquid film thickness. The thickness h is obtained by measuring the shift of the position of the image of a wire in presence of liquid (image b) with respect to its position when the mirror is dry (image a). The thickness after the jump is here $75 \pm 5\,\mu m$. This technique allows the determination of the whole profile $h(r)$, provided that the slope is small. One finds also that the thickness inside the jump is of the order of $10\,\mu m$.

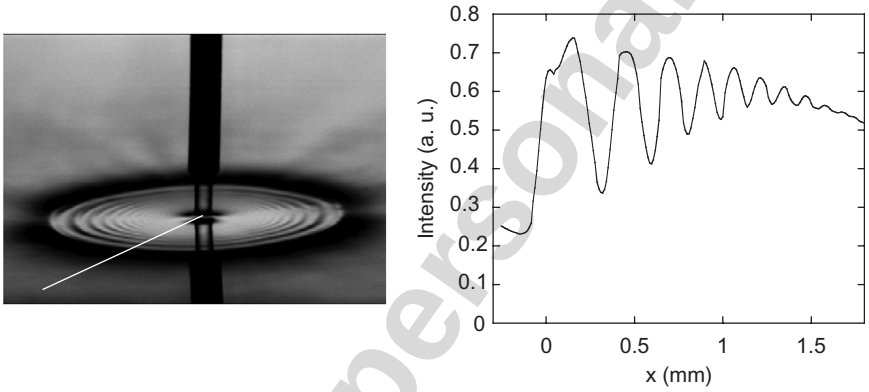

Fig. 4. Left: stationary ripples appear to grow progressively into the region inside the jump for temperatures below T_λ (here $T = 1.71\,K$). The vertical bar at the top center of the image is the filling capillary. Right: the intensity profile along the white line in the image (the origin for x is at the jump).

stable, that is at 4.2 K and medium flow rate. It is of the order of 10 μm.

The experiments are performed in the following way. First we wait until the temperature of the helium bath is stabilized, which may require 1 h. Then the gas is admitted in the filling line at a fixed flow rate Q. We wait until the temperature gradient in the fill line is stable, and record images of both the jump and the wire. Then Q is changed (non-monotonically), and we repeat the measurements. Most of our measurements have been taken in this stationary configuration, with the liquid flowing over the edge of the mirror. Once the dead volume at the bottom of the cell is filled, the outer level increases linearly with time, and the jump radius R_j starts decreasing until it ultimately collapses. We have also analyzed some of these sequences, where we can measure R_j as a function of the liquid depth d at constant flow rate. In this case, the radius is quasi-stationary: dR_j/dt is much smaller than the fluid velocity in the fast flow region, so that one expects that the velocity field is not much modified. However, this is not the case in the outer region since the velocity has to vanish at a finite distance.

At low temperatures, stationary ripples begin to grow into the region inside the jump, as shown in Fig. 4. The right side of the Fig. 4 shows the intensity profile along a cut through the image. The variation of the intensity is not due to the change of the liquid depth, but is due to the local slope of the liquid–vapor interface. Indeed, the diffusive source is seen through a small window (the numerical aperture is of the order of 0.1) so that the illumination of the entrance pupil of the lens, and hence the intensity in the image plane, depends on how much the light reflected through the film is deflected. As long as the relative variation in intensity is small, the intensity depends linearly on the local slope. This allows us to extract the decay constant from the intensity profile. Moreover, knowing the numerical aperture for both illumination and imaging, one can estimate the amplitude of the ripples, which is found to be at most 1 μm. The total liquid depth is of the order of 10 μm. More details of the analysis will be given in Section 4.

3. Radius of the jump

3.1. Models of the jump radius

Several models have been proposed to predict the value of R_j as a function of the following parameters: the volumetric flow rate Q, the jet radius a, the thickness d of the fluid outside the jump, and the fluid kinematic viscosity v. While the hydraulic jump is easy to observe, the theory is challenging because of the intrinsically two-dimensional nature of the flow, and the presence of a free boundary; it remains a problem of current interest. In the original treatment by Rayleigh [4] for an inviscid fluid, the jump is treated as a shock that connects the fast flow in the thin layer and the slow flow downstream. If the characteristics of the flows are known, conservation of mass and momentum flux set the value of R_j. Such an approach leads to the result (quoted in Watson [9]):

$$\frac{R_j d^2 g a^2}{Q^2} + \frac{g d a^4}{2Q^2} = \frac{1}{\pi^2}. \tag{1}$$

Rayleigh's expression leads to values of R_j much larger than measured experimentally. The scaling of R_j with Q rather supports a model where the viscosity plays an important role. Watson [9] derived a model in which the thin flow is divided into two regions. Close to the impact, the flow is inviscid with a growing boundary layer which invades the whole flow at $r = R_0$; for $r > R_0$ the flow is fully viscous. Watson assumes a self-similar velocity profile for $r > R_0$, approximating the radial component of the velocity by the form $u(r,z) = U(r)f(z/h(r))$, where $h(r)$ is the depth of the liquid at a distance r from the origin. The functions U and f are determined from the equations of motion and continuity. The conditions of conservation of mass and momentum conservations at the jump in this model lead now to

$$\frac{R_j d^2 g a^2}{Q^2} + \frac{a^2}{2\pi^2 R_j d} = 0.01676\{(R_j/a)^3 Re^{-1} + 0.1826\}^{-1}, \tag{2}$$

where $Re \equiv Q/va$ is the Reynolds number at the jet. Experimental data are in reasonable agreement with this prediction.

Watanabe et al. [3], on the other hand, argue that treating the jump as a discontinuity involving extra energy loss is inconsistent with the flow being stationary and laminar, which is the case at low Re. They constructed a viscous theory that produces a smooth but kink-like surface shape. They introduce a new free parameter λ in the velocity profile, which is no longer assumed to be self-similar. In a shallow water approximation, they obtain two coupled differential equations for $\lambda(r)$ and the film height $h(r)$. With two boundary conditions on h before and after the jump, numerical integration yields $h(r)$ and the velocity profile, which presents a separation bubble, or eddy, behind the jump. The jump radius is expected to be of the order of the characteristic scale r_* for the radius: $r_* = [(Q/2\pi)^5 v^{-3} g^{-1}]^{1/8}$. It was shown that R_j indeed scales roughly like r_* [10]. Note that in order to calculate the jump radius R_j with the model developed in Ref. [3], it is necessary to know the depth of the liquid inside the jump. A direct measurement is possible only in the normal phase (see Fig. 3).

Bush and Aristoff [5] recently discussed the effect of capillary forces due to the curved surface of the jump. Since the typical values of R_j are in the millimeter range, much smaller than in previous experiments, capillary effects should be more important in our experiment. Bush and Aristoff extend Watson model to include capillary forces acting at the jump. They obtain:

$$\frac{R_j d^2 g a^2}{Q^2}\left(1 + \frac{2f}{Bo}\right) + \frac{a^2}{2\pi^2 R_j d} = 0.01676\{(R_j/a)^3 Re^{-1} + 0.1826\}^{-1}, \tag{3}$$

which is the same as Eq. (2), except for the factor $(1 + 2f/Bo)$. The number f characterizes the shape of the jump; it is equal to 1 for a sharp, step-like jump, and tends to zero for very smooth jump. Setting $f = 1$ thus correspond to an upper bound for capillary forces and yields a lower bound for R_j. The Bond number Bo appears as a second parameter in the problem : $Bo \equiv dR_j/L_C^2$, where L_C is the capillary length ($L_C \equiv \sqrt{\gamma/\rho g}$, where γ is the surface tension, ρ the density and g the acceleration of gravity). As typical values of Bo in our system are much smaller than in previous experiments, Bush's approach should be easily tested in our experiment.

3.2. Measurements of the jump radius in the normal fluid

Experiments were performed at three different temperatures above T_λ (4.2, 3, and 2.4 K). The surface tension is the only physical parameter that varies significantly in this temperature range. In our setup, the control parameter is the flow rate Q. However, the height d after the jump is not imposed, and varies as a function of Q. Thus the variation of the radius as a function of Q alone is not meaningful. In Fig. 5, R_j and d are plotted as a function of the flow rate Q. For a fixed flow rate, d decreases with T between 4.2 and

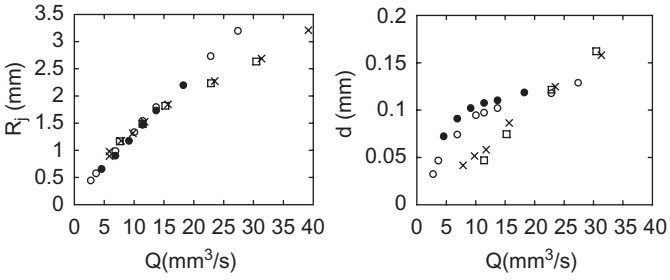

Fig. 5. Characteristics of the jump for normal fluid. Left: radius R_j as a function of the flow rate Q. Right: thickness d as a function of Q. ○ and ●: 4.2 K, ×3 K; □: 2.4 K.

3 K, and does not change between 3 and 2.4 K. Clearly, d does not depend only on the value of the surface tension. At 4.2 K, we have also observed that d depends on the thermalization of the cell with the main bath. Presumably residual thermal gradients influence the way the liquid falls over the edge of the mirror.

Since we measure both Q and d, it is possible to compare the measured value of R_j with the prediction by Watson. Eq. (2) is easily solved numerically. In Fig. 6, we have plotted the predicted value of R_j as a function of the measured R_j in Watson's model (open symbols). The order of magnitude is correct, but there is a clear discrepancy; the predicted value is generally higher than the measured one. At fixed R_j, the lower the temperature, the higher the prediction. As the surface tension is the only parameter which varies significantly, capillary effects are the natural candidate to explain the disagreement. For the smallest jump in our experiment, we find that Bo is about 0.2, which means that capillary forces are more than a small correction! Hence we also plot the solution of Eq. (3) in the limit of an abrupt jump ($f = 1$), shown as solid symbols in Fig. 6. The model of Bush and Aristoff collapses the data much better than Watson's; the predicted values in this model are now systematically smaller than the measured ones but this is expected since they are computed in the limit $f = 1$, which correspond to a lower boundary for R_j. Real jumps, especially at low flow rate (i.e. small radii) look very smooth. A precise comparison with Bush and Aristoff predictions requires determining the actual profile of the jump. Unfortunately, our optical techniques do not work when the local slope is large, which happens precisely at the jump.

At this stage, it seems that treating the jump as a discontinuity provides a good estimate of R_j. This is slightly surprising in view of the image in Fig. 3, where the jump is smooth and the flow is quite laminar. Such situations, which require a very accurate temperature regulation, are obtained only for $T = 4.2$ K and $Q \lesssim 10\,\mathrm{mm}^3/\mathrm{s}$. For these jumps, we have compared experimental data with the model developed by Bohr and co-workers [3]. In order to obtain a prediction for R_j, one needs to numerically integrate the coupled equations for the interface height $h(r)$ and the velocity profile from a point r_1 inside the jump to a point far downstream, where $h = d$. The thickness $h(r_1)$ is about 10 μm. Following the integration method proposed by Watanabe et al., we obtain $R_j \simeq 0.95 r_*$, with $r_* = [(Q/2\pi)^5 \nu^{-3} g^{-1}]^{1/8}$ (the numerical factor is not very sensitive to the value of $h(r_1)$). This yields values roughly two times larger than the experimental one. Thus Bohr's model does not seem to describe accurately small jumps. One first reason could be that capillary forces are neglected. According to Watanabe et al., capillarity is negligible if the Weber number $We \equiv L_C^2/r_*^2$ is small. For $Q \sim 10\,\mathrm{mm}^3/\mathrm{s}$, one finds $We \sim 0.25$ so that capillarity forces are small but not negligible as in Bohr's approach. A second reason could be that R_j is not very large compared to R_0, the point where the velocity profile changes from a Blasius type to a fully viscous profile. From Watson [9], one finds that in our experiments $R_j \gtrsim 2R_0$.

3.3. Going through the superfluid transition

In order to study what happens at the superfluid transition ($T_\lambda = 2.17$ K), we have set the flow rate at a constant value $Q = 17\,\mathrm{mm}^3/\mathrm{s}$ and slowly decreased the temperature through the transition at a rate of 30 mK/min. Images are shown in Fig. 7. There is little change in the jump radius on passing through the transition temperature.

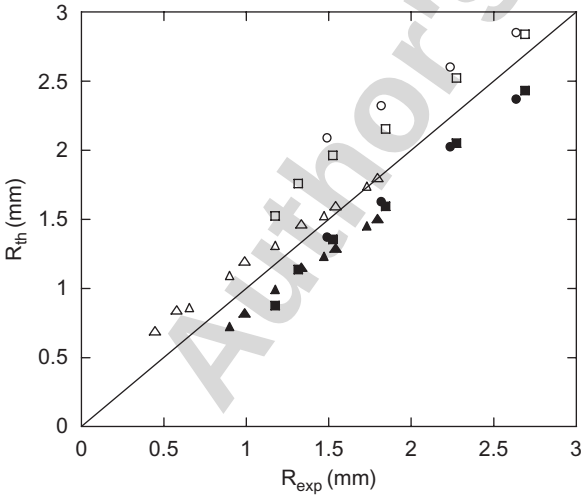

Fig. 6. Comparison of the measured jump radius R_j with the prediction without surface tension [9] (open symbols) and with surface tension in the abrupt-jump limit [5] (closed symbols) Circles: 2.45 K; squares: 3.0 K; triangles: 4.25 K. Neglecting the surface tension yields too large a radius, but in the abrupt-jump limit, capillary forces are overestimated.

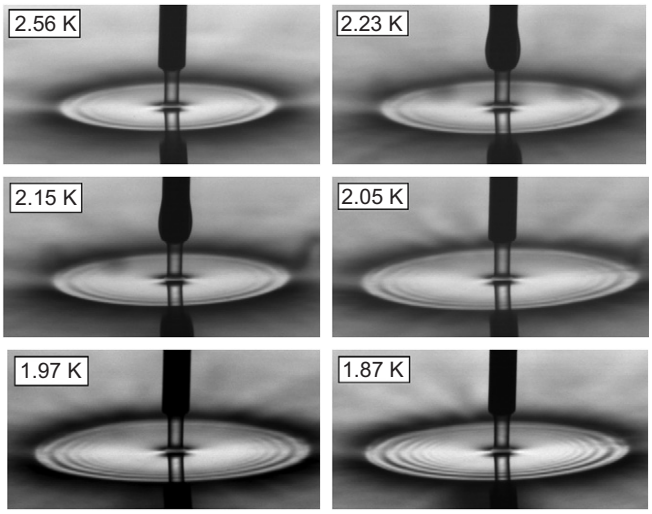

Fig. 7. Evolution of the jump as a function of the temperature: R_j varies only slightly at the superfluid transition. Ripples appears progressively below T_λ. $Q = 17\,\mathrm{mm}^3/\mathrm{s}$ and $R_j \simeq 2$ mm.

This is quite surprising: from the Eq. (1), which is expected to be relevant for a non-viscous fluid, one expects the radius to increase roughly by a factor 10. Other measurements at 1.5 K at various flow rate have confirmed that the radius is roughly independent of the nature of the fluid.

We propose the following explanation. Below T_λ, the liquid can be considered as a mixture of a normal and a superfluid component (a comprehensive description of the behavior and properties of superfluid helium can be found in Wilks [11]). In this two-fluid model, only the superfluid has zero viscosity and zero entropy, while the normal component carries the entropy and has a finite viscosity η_n which decreases roughly by a factor 2 when T decreases from T_λ down to 1.5 K. Depending on the boundary conditions, the superfluid component may flow independently of the normal component, or together with it. Only in the first case may the flow be truly non-dissipative.

Moreover, it is well known that the flow of the superfluid component itself can be dissipative if the velocity exceeds a critical value U_C which depends mainly on the thickness (or more generally on the transverse dimension) of the flow (see Ref. [11, pp. 383ff.]). The dissipation mechanism is not completely understood, but there is a consensus that quantum vortices are generated if the velocity is larger than U_C. In our setup, vortices may be generated in the tube, where Re is of the order of a few thousand (assuming that the effective kinematic viscosity is of the order of η_n/ρ), or where the jet impacts the substrate and the direction of the flow is turned outwards. As seen in Fig. 7, the presence of ripples inside the jump blurs the image of the wire and make a direct measurement of the liquid thickness impossible. However, the thickness is mainly set by the jet diameter, and it should still be of the order of 10 μm when the liquid is superfluid. For such a thickness, the critical velocity is of the order of 10 cm/s [11]. This is precisely the order of magnitude of the velocity at the jump, so that the flow is presumably dissipative inside the jump, and the generation of vortices may also occur in the thin film region. For temperatures above 1.5 K, the normal fraction is larger than 0.1. Because of the mutual friction between the vortices and the normal component, the two components "lock" to each other. Then, as a first approximation, the superfluid behaves as an ordinary fluid with an effective kinematic ν_{eff} of the order of η_n/ρ. For instance, grid turbulence experiments yields ν_{eff} roughly twice as large as η_n/ρ at $T = 1.5$ K [12]. The exact value of ν_{eff} may depend on Re and on the geometry of the flow. As the simplest guess, we will suppose in the following that $\nu_{\text{eff}} = \eta_n/\rho$.

3.4. Jump radius at 1.5 K

We have performed measurements of both the jump radius R_j and the fluid thickness d for various flow rates at $T = 1.5$ K. In Fig. 8, we compare the measured value for R_j with the predicted values in Watson's model and in Bush's model. With the hypothesis $\nu_{\text{eff}} = \eta_n/\rho$, one finds that the data in the superfluid regime collapse well with the data in the normal regime. This supports the idea that the fluid behaves as if it were a usual viscous fluid, at least for the jump radius. One should note that the predictions for R_j is not very sensitive to the exact value of ν_{eff}: an increase of ν_{eff} by a factor two leads to a decrease of R_j by only 15%.

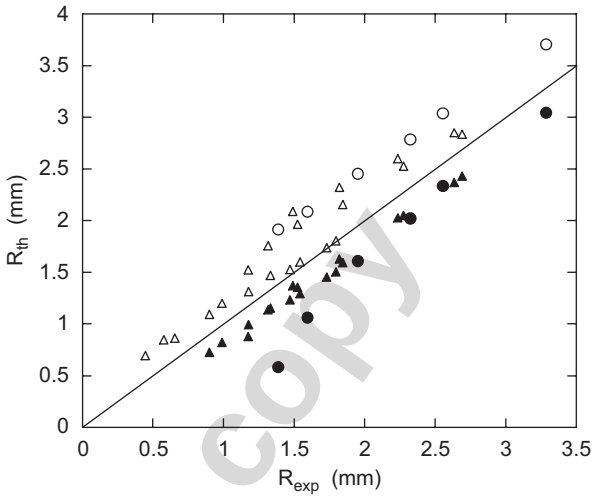

Fig. 8. Comparison of the measured jump radius R_j with the prediction without surface tension [3] (open circles) and with surface tension [5] (closed circles). The triangles correspond to the data for the normal fluid (cf Fig. 6).

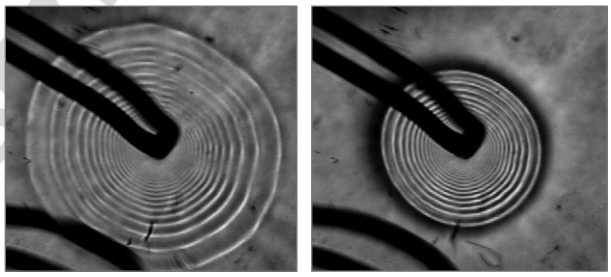

Fig. 9. Collapse of the jump at $T = 1.5$ K as the outer level d increases ($Q = 26.67\,\text{mm}^3/\text{s}$). Left: $d = 122\,\mu\text{m}$ and $R_j = 3.30$ mm. Right: $d = 283\,\mu\text{m}$ and $R_j = 1.83$ mm.

Data in a wider range of d can be obtained when looking at the filling of the cell: when the dead volume below the plate is filled by liquid, the outer level d starts to increase. This makes the jump radius decrease, as seen in Fig. 9.

As R_j decreases slowly ($\mathrm{d}R_j/\mathrm{d}t$ is much smaller than the fluid velocity inside the jump), one expects than R_j can adjust to slowly varying boundary condition. In this way, one can measure R_j as a function of d, at constant flow rate Q. Data are shown in Fig. 10, together with the predictions corresponding to the model by Watson, and with the model including a correction for the surface tension. Once again, experimental data fall within the two predictions. Looking more closely at the data, it is clear that the data are closer to the prediction which takes into account capillary forces. This is consistent with the observation that the jump becomes steeper as R_j decreases.

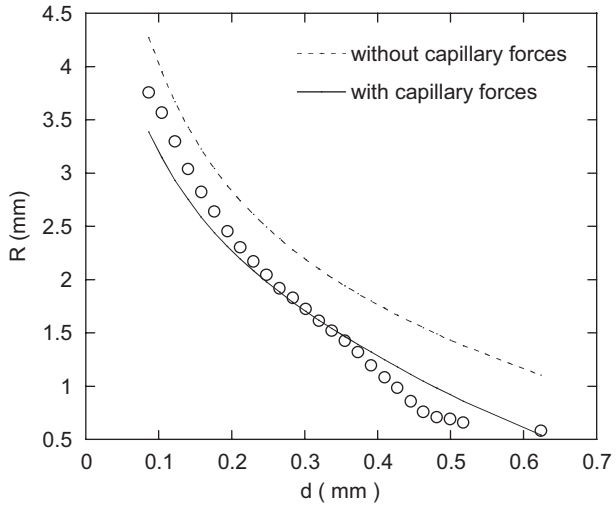

Fig. 10. Variation of the jump radius R_j as a function of the outer fluid thickness d ($Q = 26.67\,\mathrm{mm}^3/\mathrm{s}$, $T = 1.5\,\mathrm{K}$).

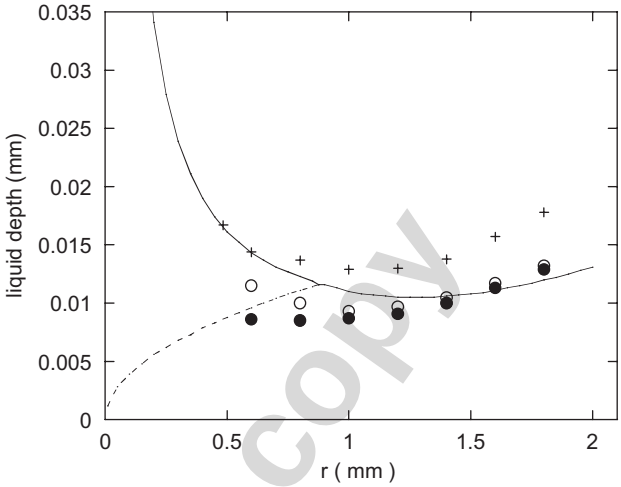

Fig. 11. This figure shows $h(r)$ according to the Watson model (full line). The dashed line represents the limit of the boundary layer invading the liquid from the substrate. The data points are computed from the measurement of the wavelength of the ripples and the use of either Eq. (4) (+), or Eq. (5) (○: full calculation, •: boundary layer approximation). The final uncertainty on h is of the order of $\pm 1.5\,\mu\mathrm{m}$. Here the temperature is $T = 1.5\,\mathrm{K}$ and the flow rate $Q = 15.24\,\mathrm{mm}^3/\mathrm{s}$.

4. Ripples in the fast flow region

Above the superfluid transition, a few ripples are visible close to the jump. The most striking feature of the flow below T_λ is the increasingly large number of ripples that are visible within the jump, as seen in Fig. 7.

These ripples are stationary, which means that they are traveling upstream with respect to the flow of the liquid. It is observed that the phase of the ripples is independent of the radius of the jump. This suggest a method for measuring the depth of the liquid inside the jump, when it is too shallow or too curved to measure by means of the image of the wire, for the wavelength λ should depend on $h(r)$. We start from the assumption that $h(r)$ varies slowly enough that it makes sense to speak of the wavelength at a particular radius r, and that it is given by the distance between wave crests in the image. We also treat the waves as plane waves, rather than circular waves: this approximation is justified by the fact that we do not observe any ripples at radius small compared to λ.

To proceed, from the wavelength, we determine the wave number $k = 2\pi/\lambda$. As a first approximation, we note that since the waves are stationary in the reference frame of the laboratory, in the reference frame moving with the average velocity $\langle U\rangle$ of the fluid, they are traveling upstream with an equal and opposite velocity. Thus their phase velocity $v_\phi \equiv \omega/k$ is equal to $\langle U\rangle$ (here ω is the frequency of the waves in the fluid frame of reference). $\langle U\rangle$ depends on r and $h(r)$ by the equation of continuity, $Q = 2\pi r h(r)\langle U(r)\rangle$. The dispersion relation for waves in a shallow liquid is [13, p. 240]:

$$\omega^2 = (gk + \gamma k^3/\rho)\tanh kh. \tag{4}$$

This set of equations can be solved numerically for the depth of the liquid, $h(r)$. The result is in reasonable agreement with the prediction of Watson [9], as shown in Fig. 11, which lends credence to the procedure. It cannot be compared with a direct measurement, since the image of the wire is blurred because of the oscillation of the interface. However, in our parameter range, the minimum thickness is only weakly dependent on the viscosity, so that one expects the value of h to be set by the jet radius, and to be still of the order $10\,\mu\mathrm{m}$. This value is consistent with the one obtained from the simple analysis of the ripples.

Although we did not observe the growth of the ripples in the time domain, the dispersion relationship given by Eq. (4) suggests that the group velocity of the waves, $v_g = \mathrm{d}\omega/\mathrm{d}k$ in the fluid frame of reference is greater than the average fluid velocity $\langle U\rangle$, so we might expect that the disturbance represented by the ripples grows upstream (i.e., though the crests remain stationary, new crests will form upstream during the initial growth of the perturbation). It has been suggested by Volovik [14] that the ripples are generated by interactions with the substrate, which would generate stationary waves (the perturbation due to the surface has $\omega = 0$ in the laboratory frame of reference). It is interesting to note that there is a minimum fluid velocity below which stationary ripples cannot exist, $\langle U_{\min}\rangle = \min(\omega(k)/k)$ (here $\omega(k)$ is in the fluid frame of reference). This same criterion is required for the hydraulic jump to exist in Rayleigh's inviscid model, and it is the same as the Landau criterion for the creation of quantum excitations in a fluid moving past a wall, as noted by Volovik. In our experiment, however, because the film is thin compared to the capillary length, the minimum velocity is zero and stationary capillary waves may form for any fluid velocity.

To establish the relationship between λ and h more accurately, and to determine the relationship between the viscosity ν of the liquid and the spatial dependence of the ripple amplitude, we turn to the Navier–Stokes equations

and look for solutions that correspond to stationary ripples. We consider the region where the boundary layer has reached the surface, so that the steady background velocity of the liquid has a Poiseuille profile: $\vec{U}(z) = U_0(h-z)^2\hat{x}$. (The direction of the flow is $\hat{x}$; the vertical direction is $\hat{z}$; we still consider plane flows rather than circular flows; U_0 is the velocity at the free surface, and $\langle U\rangle = \frac{2}{3}U_0$.) We look for small amplitude perturbations of this flow, of the form $\vec{v} = \vec{U}(z) + u(x,z)\hat{x} + w(x,z)\hat{z}$, we look for periodic perturbations proportional to $e^{i(kx-\omega t)}$, and we linearize in terms of the small perturbations u and w. Note that k may be complex. If we write $k = K + i\kappa$, where K is the real part and κ the imaginary part, then K determines the wavelength of the ripples, and κ governs the amplitude variation. Experimentally, κ can be determined from the decay of the ripples with distance from the jump in the intensity profile of the reflected light in the image (see Fig. 4).

The Navier–Stokes equations reduce, in the approximation described above, to the famous Orr–Sommerfeld equation (for a derivation, see Ref. [15, p. 156]), with $\omega = 0$ since the ripples are stationary in the lab frame:

$$\frac{1}{ikRe}\left(\frac{\partial^2}{\partial z^2} - k^2\right)^2 \phi = U(z)\left(\frac{\partial^2}{\partial z^2} - k^2\right)\phi - U''(z)\phi. \tag{5}$$

Here ϕ is the velocity potential; $u(x,z) = \phi'(z)e^{i(kx-\omega t)}$, $w(x,z) = -ik\phi(z)e^{i(kx-\omega t)}$.

The boundary condition at the lower surface is the non-slip condition, $u(0) = w(0) = 0$, which means $\phi(0) = \phi'(0) = 0$.

The boundary conditions at the upper surface are continuity of the normal and tangential stress, which must include the effects of surface tension. These can be written, after linearization (see for instance [16–18]):

$$-k\phi'(h) + \frac{i}{Re}(3k^2\phi'(h) - \phi'''(h)) + k\left(\phi(h) + \frac{k^2}{Bo}\right)\frac{\phi(h)}{Fr} = 0 \tag{6}$$

and

$$\phi''(h) + (k^2+2)\phi(h) = 0. \tag{7}$$

Here, the Bond number is $Bo = \rho g h^2/\sigma$ (not the same as defined in Section 3.1) and the Froude number is $Fr = U_0^2/hg$. This system of equations may be solved numerically by two methods, shooting, and the boundary layer approximation. (The Orr–Sommerfeld equation has also been studied in the context of the hydraulic jump by Cholemari [8], who use the self-similar velocity profile of Watson instead of the Poiseuille flow for the unperturbed flow; in order to study the stability of the jump, they seek solutions with real k and complex ω.)

In the shooting method, we integrate the Orr–Sommerfeld equation numerically, either by power series or by fourth-order Runge–Kutta, with the initial conditions $\phi(0) = \phi'(0) = \phi''(0) = 0$ and $\phi'''(0) = 1$, or $\phi(0) = \phi'(0) = \phi'''(0) = 0$ and $\phi''(0) = 1$ (both of which satisfy the boundary condition at $z = 0$). If these two solutions are called ϕ_1 and ϕ_2, then the general solution is of the form $\phi = A\phi_1 + B\phi_2$. The boundary conditions at the free surface, Eqs. (6) and (7), then reduce to two linear equations in A and B; if A and B are not both to be zero, Eqs. (6) and (7) must not be linearly independent of each other. This is true only for particular values of k, yielding k as a function of h.

In the boundary layer approximation [3], since the vertical scale of the problem is much smaller than the horizontal scale, intertial, pressure and viscous terms are all retained, but terms with derivatives with respect to x are neglected compared to terms with derivatives with respect to z. As a result, the pressure can be determined immediately, and the Orr–Sommerfeld equation is replaced by a third-order integro-differential equation,

$$-U(z)\phi'(z) + U'(z)\phi(z) = -\frac{1}{We}k^2\phi(h) + \frac{i}{kRe}\phi'''(z) \tag{8}$$

with boundary conditions $\phi(0) = \phi'(0) = \phi''(h) = 0$. The Weber number is $We = BoFr$.

Integrating from $z = 0$ using the first two boundary conditions leads to the third boundary condition becoming an implicit equation for k.

The results of the two methods of solution, shooting and boundary layer, are quite close; and the result for the real part of k is not very different from the naive model represented by Eq. (4), shown in Fig. 11 to be in reasonable agreement with the model of Watson [9]. Since this model is based on the classical hydrodynamics of a viscous fluid, this result suggests as far as $h(r)$ goes, the liquid is behaving like a normal viscous liquid with a viscosity comparable to the viscosity of the normal component of the fluid.

Fig. 12a shows that κ is about 20% below the predicted value above the lambda temperature. However, the disagreement becomes much worse below the lambda transition. In fact, between 1.7 and 2.0 K, where the viscosity of the normal fluid η_n changes by 10%, κ *decreases by a factor of 2*, as shown in Fig. 12b. Therefore, something else must be changing in this temperature range, causing the variation in κ. One possibility is the normal fluid fraction ρ_N/ρ. In Fig. 12c, we show κ as a function of the normal fluid fraction. The data above the lambda transition collapse to a point (the normal fluid faction is 1, above T_λ), but below T_λ, it appears that κ is approximately proportional to the normal fluid fraction.

5. Conclusion

In conclusion, then, we find that models of the hydraulic jump that treat it as a shock do an adequate job of predicting the radius of the jump, especially when the effects of the surface tension at the curved surface of the jump is taken into account. The model of Watanabe et al. [3] (which does not include surface tension) is less accurate (as one would expect) for small jump radii.

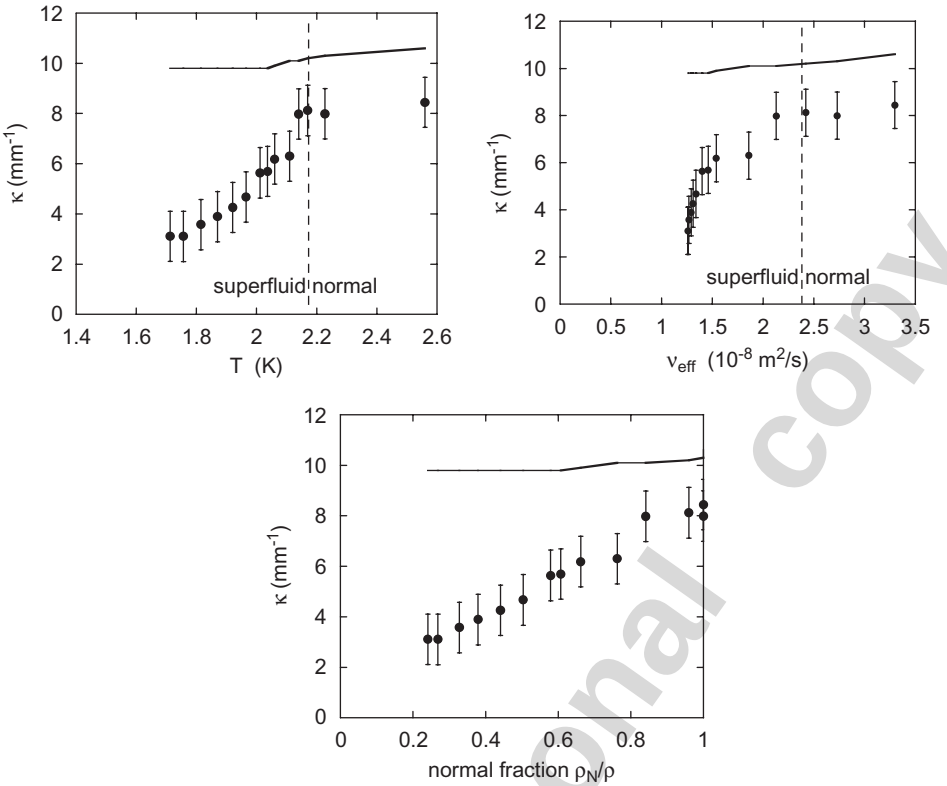

Fig. 12. The growth coefficient κ plotted as a function of temperature, effective viscosity $v_{\text{eff}} = \eta_N/\rho$, and normal fluid fraction (dots: experimental data, full line: obtained from the resolution of the Orr-Sommerfled equation). Above T_λ the calculation of κ disagree with experiment by about 20%, but below T_λ, the discrepancy is great. The variation of κ below T_λ cannot be explained by the variation of the effective viscosity; it appears to be proportional to the fraction of the normal component ρ_N/ρ.

Below the superfluid transition temperature, the jump radius and the depth profile $h(r)$ appear to behave as though the fluid is normal. This is not entirely surprising, in view of the fact that the velocity of the fluid in the incoming jet and inside the jump exceeds the critical velocity for superfluidity.

The damping of the ripples tells a different story, however. Above T_λ, the growth of the ripples is within 20% of the prediction of a model of a classical viscous fluid. However, below T_λ the damping deviates markedly from the classical model, but appears to be proportional to the normal fluid fraction. One might imagine that the ripples represent an oscillation of the superfluid decoupled from the normal fluid, such as occurs in the case of third sound or fourth sound, where the normal component is held in place by friction with a substrate or a narrow pore, respectively [11, p. 421] but the superfluid is free to oscillate. However, if the fluid is normal, on account of its being over the critical velocity, then mutual friction between the vorticity in the normal fluid and the superfluid components should lock them together, and it should not be possible for the superfluid to oscillate independently. (Moreover, as in the case of third and fourth sound, one might expect the wave velocity to be very dependent of ρ_N/ρ, and hence on the temperature. This is not observed: the wavelength varies very little with the temperature.)

Another possible explanation for the discrepancy in the damping of the waves is that in the case of supercritical velocity, the effective viscosity is not equal to η_n/ρ. Available data at large Re for homogeneous turbulence leads to v_{eff} roughly twice η_n/ρ, which makes the discrepancy worse [12]. In order to reconcile our experimental data with the flow of an ordinary viscous fluid, one need the effective viscosity to decrease very strongly when T decreases, which seems unlikely.

Using data from grid turbulence experiments, one may try to estimate the amount of vorticity in the film. Supposing that the decay time is taken to be 1 ms, which is the order of magnitude of the time for the liquid to fall from the tube, and extrapolating the data for grid turbulence at $Re = 10^4$ [19], one finds that the vortex line length L par unit volume is of the order of $L \sim 4 \times 10^{10}\,\text{m}^{-2}$. This leads to an average distance between vortices of the order of 5 μm, which is comparable to the depth of the liquid. In this case, it may not be valid to treat the fluid as homogeneous to begin with.

Ultimately, the nature and the origin of the ripples below T_λ remains an open and interesting question.

Acknowledgments

We thank Sébastien Balibar, Grigori Volovik and Joe Vinen for useful discussions. One of us (M.S. Pettersen)

gratefully acknowledges the support of the Université Paris 7 which enabled him to participate in this work.

References

[1] B.L. Blackford, Am. J. Phys. 64 (1996) 164.
[2] Y. Brechet, Z. Néda, Am. J. Phys. 67 (1999).
[3] S. Watanabe, V. Putkaradze, T. Bohr, J. Fluid Mech. 480 (2003) 233.
[4] L. Rayleigh, Proc. R. Soc. A90 (1914) 324.
[5] J.W.M. Bush, J.M. Aristoff, J. Fluid Mech. 489 (2003) 229.
[6] E. Rolley, C. Guthmann, C. Chevalier, M. Pettersen, AIP Conf. Proc. 850 (2006) 141.
[7] R.J. Donnelly, C.F. Barenghi, J. Phys. Chem. Ref. Data 27(1) 1217.
[8] M.R. Cholemari, J.H. Arakeri, Phys. Fluids 17 (2005) 084108.
[9] E.J. Watson, J. Fluid Mech. 20 (1964) 481.
[10] T. Bohr, P. Dimon, V. Putkaradze, J. Fluid Mech. 254 (1993) 635.
[11] J. Wilks, Properties of Liquid and Solid Helium, Oxford, 1987.
[12] S. Stalp, J. Niemela, W. Vinen, R. Donnelly, Phys. Fluids 14 (2002) 1377.
[13] L.D. Landau, E.M. Lifshitz, Fluid Mechanics, Pergammon, Oxford, 1979.
[14] G.E. Volovik, Pis'ma ZhETF 82 (2006) 706 (JETP Lett.).
[15] P.G. Drazin, W.H. Reid, Hydrodynamic Stability, Cambridge, 2004.
[16] T.B. Benjamin, J. Fluid Mech. 2 (1957) 554.
[17] F.H. LeBlond, F. Mainardi, Acta Mech. 68 (1987) 203.
[18] M.K. Smith, J. Fluid Mech. 217 (1990) 469.
[19] L. Skrbek, J. Niemela, R. Donnelly, Phys. Rev. Lett. 85 (2000) 2973.